Magnetically switchable mechano-chemotherapy for enhancing the death of tumour cells by overcoming drug-resistance

Chenyang Yao [a,b,1], Fang Yang [a,c,*,1], Li Sun [a,1], Yuanyuan Ma [a], Stefan G. Stanciu [d], Zihou Li [a], Chuang Liu [a], Ozioma Udochukwu Akakuru [a,b], Lipeng Xu [a], Norbert Hampp [c], Huanming Lu [a], Aiguo Wu [a,*]

[a] Cixi Institute of Biomedical Engineering, CAS Key Laboratory of Magnetic Materials and Devices & Zhejiang Engineering Research Center for Biomedical Materials, Ningbo Institute of Materials Technology and Engineering, Chinese Academy of Sciences, 1219 ZhongGuan West Road, Ningbo 315201, China
[b] Center of Materials Science and Optoelectronics Engineering, University of Chinese Academy of Sciences, Beijing, 100049, China
[c] Fachbereich Chemie, Philipps Universität Marburg, Marburg, 35032, Germany
[d] Center for Microscopy-Microanalysis and Information Processing, University Politehnica of Bucharest, Bucharest 060042, Romania

ARTICLE INFO

ABSTRACT

The emergence of drug-resistant tumour cells significantly interferes with the effectiveness of chemotherapeutic treatment plans and represents a major obstacle in the ongoing quest to overcome cancers. Therefore, exploring in detail new therapeutic strategies that can obviate this important challenge is regarded as a very important topic at the time being. Herein, we propose a non-invasive and remotely controllable mechano-chemotherapeutic approach that relies on the use of a rotating magnetic field (RMF) of low intensity (45 m T) in combination with a therapeutic agent consisting of a composite nanomaterial comprised of a poly(lactic-co-glycolic acid) (PLGA) shell co-loaded with $Zn_{0.2}Fe_{2.8}O_4$ magnetic nanoparticles (mNPs) and Doxorubicin (DOX). We show that RMF exposure induces a mechanical movement to this nanomaterial, which can be exploited for (i) controllably releasing the anti-cancer drug for chemotherapy, and (ii) promoting the death of tumour cells by means of mechanical forces exerted onto their membranes. Such dual behavior leads to combating cancer cells via different and complementary routes enabling a controllable and efficient therapy. The proposed model enables controllable tumor therapy by precisely operating the magnetic nanomaterials at the nanometer scale, and its applicability is neither restricted to the nanomaterial here demonstrated nor to solely addressing cancer. Modified variants of the proposed model, together with the corresponding therapeutic agents, can be developed to address other pathologies, enabling novel therapeutic approaches that exceed the precision and efficiency of current ones.

© 2020 Elsevier Ltd. All rights reserved.

Introduction

Chemotherapy is one of the most common methods to cure cancers or slow down their progression [1]. However, the ability of tumor cells to develop drug resistance over time currently represents one of the major constraints of such therapeutic strategies [2]. These aptitudes of the tumor cells to learn how to evade and protect themselves from drugs make the design of generally applicable treatment plans almost impossible [3], and impose the need for personalized approaches whose design and implementation is difficult and expensive. As a result of this situation, significant focus has been placed over the past years on the development of physical methods capable to overcome drug resistance [3]. In this quest, optical and electrical approaches have been designed to fight resistant cells, but limitations such as: invasive mode of stimulation, excessive action area, and slow switch kinetics keep these solutions from becoming widely used. An alternative way of tackling drug-resistant cells relies on magnetic techniques which are already used in many other fields of medicine as a result of their huge advantages, such as deep penetration into biological tissues with negligible attenuation and precisely controllable operation, by means of magnetic fields that can be used remotely and non-invasively.

* Corresponding author at: Cixi Institute of Biomedical Engineering, CAS Laboratory of Magnetic Materials and Devices & Zhejiang Engineering Research Center for Biomedical Materials, Ningbo Institute of Materials Technology and Engineering, Chinese Academy of Sciences, 1219 ZhongGuan West Road, Ningbo 315201, China.
E-mail addresses: yangf@nimte.ac.cn (Y. Fang), aiguo@nimte.ac.cn (W. Aiguo).
[1] These authors contributed equally to this work.

Magnetic treatments based on magnetic nanoparticles (mNPs), rely on the fact that magnetic energy can be transformed to other forms of energy, with potential for implementing various therapies. For example, magnetothermal [4] and magnetomechanical effects [5–7] resulting from such energy transfer processes in the case of various types of functionalized materials have been demonstrated successfully to date in association with cancer. In this work, we introduce a novel mechano-chemotherapy with dual-role: i) it can carry and controllably release anti-cancer drugs used for chemotherapy by magnetic switch and ii) it is capable of exhibiting magnetomechanical effects that can promote tumor cell death.

In general, magnetomechanical materials proposed for fighting tumor cells transfer their magnetic energy to mechanical motive energy when exposed to a magnetic field. By applying the resulted mechanical force on cancer cells, their destruction is achieved. The efficiency of such approaches in terms of killing malignant cells and curing tumors, has been demonstrated in valuable efforts, relying on the application of low-frequency magnetic fields to induce the required mechanical effect [6–8]. For example, Cho et al. successfully explored a pathway leading to cell apoptosis using magnetically switchable mNPs [9]. Also, Cheng et al. found that plasma and lysosomal membrane of tumor cells can be mechanically ruptured by cell apoptosis and necrosis using their mNPs [7]. In another important study reported by Chu et al., it was shown that a magnetomechanical force with minimum 6.19 pN and maximum 35.79 pN upon a 400 m T magnetic field can significantly damage tumor cells [6].

Magnetic materials have also been used as drug-carriers. For therapeutic application, magnetic particle-based actuation is a valuable approach for controlling the release of the agent, owing to its advantages including non-invasion, safety, and simplicity. Magnetically triggered release is more efficient compared to pH- and redox-induced carrier self-opening [10,11]. Materials that rely on these latter strategies face important limitations since they cannot be controlled by an external stimulus. Consequently, although they can be functionalized to easily adsorb loads, they cannot effectively release them, at the desired time-point or location. For instance, a material, obtained by the association of Fe_3O_4 mNPs and an anti-cancer drug doxorubicin (DOX) was shown to be capable of accumulating the drugs by electrostatic attraction [12,13], but the authors faced difficulties in achieving an efficient function for controlled release.

As briefly described before, magneto-responsive materials can be triggered to release the drugs that they carry, and exhibit/exert a mechanical force onto objects they interact with through magneto-induction. In this work, we exploit these two aspects in-tandem, and consequently propose a magnetic nanomaterial that can be: i) effectively used for controlled drug-release non-invasively and remotely, by magnetic triggering, and ii) can be made by means of external magnetic fields to exhibit a mechanical force that can kill cells (irrespective of whether they are drug resistant or not). Such dual, mechano-chemotherapeutic behavior of the proposed nanomaterial leads to an enhanced therapeutic effect, as cancer cells are attacked by two complementary routes/strategies. The synthesized nanomaterial with controllable mechano-chemotherapeutic functionalities, can overcome drug resistance, consequently enhancing the death of tumour cells, using a magnetic switch as shown in Fig. 1. In previous experiments, it was shown that the co-loading of polymeric shells with superparamagnetic NPs and DOX results in very efficient theranostic agents that exhibit MRI contrast, and chemotherapeutic effects [14]. However, an important limitation of such agents consists in their ability to deal with drug-resistant cells. In this work, we demonstrate that other properties of nanomaterials exhibiting such structure (polymer shell co-loaded with mNPs and drugs) can be exploited in the purpose of overcoming tumor drug-resistance. In particular, we show that by exposing a DOX-$Zn_{0.2}Fe_{2.8}O_4$-PLGA agent to a tunable rotating magnetic field, a magnetomechanical force is exhibited by the embedded mNPs, which inflicts damage in drug-resistant tumor cells, finally leading to their death. Thus, such therapeutic agents with dual role combat cancer cells via different but complementary routes enabling more efficient and generally applicable therapies.

The proposed therapeutic agent consists in a composite nanomaterial with a poly(lactic-co-glycolic acid) (PLGA) shell that is co-loaded with $Zn_{0.2}Fe_{2.8}O_4$ mNPs and Doxorubicin (DOX), a chemotherapy medication used to treat various types of cancers, including breast cancer, lung cancer, bladder cancer, lymphoma, and acute lymphocytic leukemia. The superb properties of $Zn_{0.2}Fe_{2.8}O_4$ mNPs for MRI imaging, demonstrated in our previous work [15], confer to the proposed DOX-$Zn_{0.2}Fe_{2.8}O_4$-PLGA material valuable potential for theranostics, which however, will not be discussed in this article in order not to divert focus. In such applications, the proposed composite nanomaterial exhibits low toxicity and appreciable stability due to the high biocompatibility and stability of the PLGA shell, which confers it long-term stability. Its filling enables efficient therapeutic action, by two complementary routes, which we demonstrated in the case of MCF-7 and DOX-resistant MCF-7 (MCF-7/ADR) cells (ADR). Our experiments demonstrate that the proposed mechano-chemotherapeutic strategy enables safe and reliable controlled drug release, and can efficiently overcome drug resistance, resulting in the death of tumor cells irrespective of potential drug-eluding properties that they might exhibit.

For magnetic switching, required by the functionality of the proposed nanomaterials, we used a novel equipment capable of generating tunable rotating magnetic field (RMF), which can initiate a controllable magnetomechanical force. The underlying principles of this equipment are described theoretically, and its functionality is demonstrated experimentally in association with the proposed magnetic nanomaterial. Two important features of the proposed system are: (i) the strength of the applied magnetic field is much lower compared to the hazard value in humans [16]. (ii) by enabling a precise quantification of the magnetomechanical force, it can enable the implementation and evaluation of various other therapies based on magnetomechanical effects. In order not to divert focus, more details about this equipment are presented in the Supporting Information (SI).

The operation principles of the proposed therapeutic agent (in combination with the newly reported equipment for magnetic control) are as follows: an external RMF yielded by the proposed system with the help of two permanent magnets actuated by a rotating motor is applied to control the adsorption and release of DOX. Under the thus generated low frequency RMF, the drug molecules desorb from the composite nanomaterial triggered by the magnetomechanical force. At the same time, the applied magnetic field can be adjusted to induce a motion to the $Zn_{0.2}Fe_{2.8}O_4$ mNPs, which results in a mechanical action that inflicts to the tumor cells a stress that is incompatible with their viability. We demonstrate this mode of operation in an experiment where magnetic manipulation of the proposed material is exploited for achieving the desired novel mechano-chemotherapeutic effect leading to the death of tumour cells, irrespective of their drug-resistance abilities.

Results and discussion

Fabrication and characterization of DOX-$Zn_{0.2}Fe_{2.8}O_4$-PLGA

Superparamagnetic zinc-doped iron dioxide ($Zn_{0.2}Fe_{2.8}O_4$) NPs with valuable magnetic properties were synthesized based on a protocol that we previously developed [17,18]. Important properties of these mNPs, such as size distribution (ca. 6.6 nm), saturation
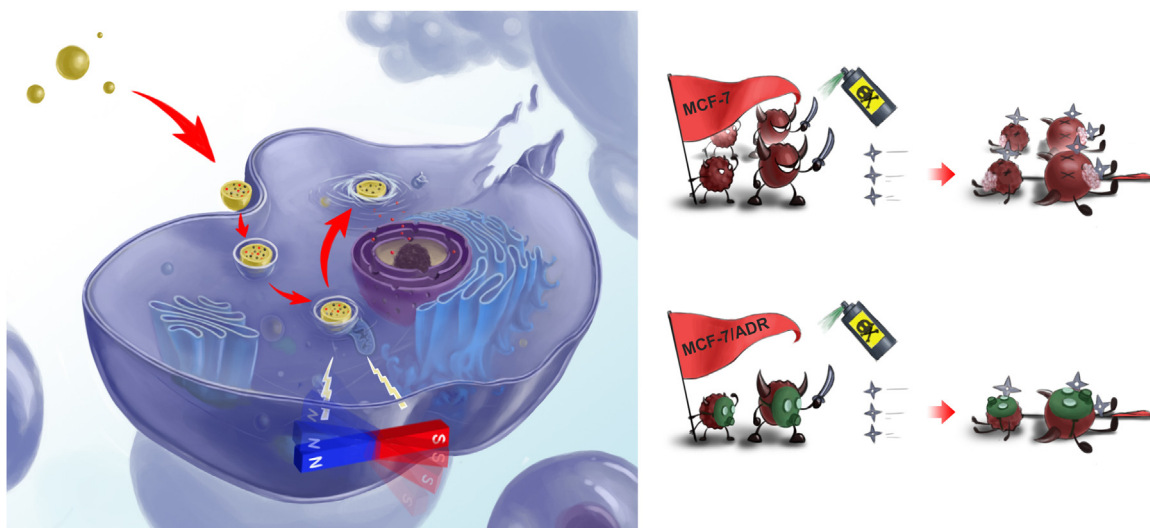
Fig. 1. Illustration of the dual therapeutic effect of the proposed nanomaterial. Mechanotherapy and chemotherapy complement each other, and their combined use yields good efficiency in terms of "killing" tumor cells irrespective of whether they are drug-resistant or not.
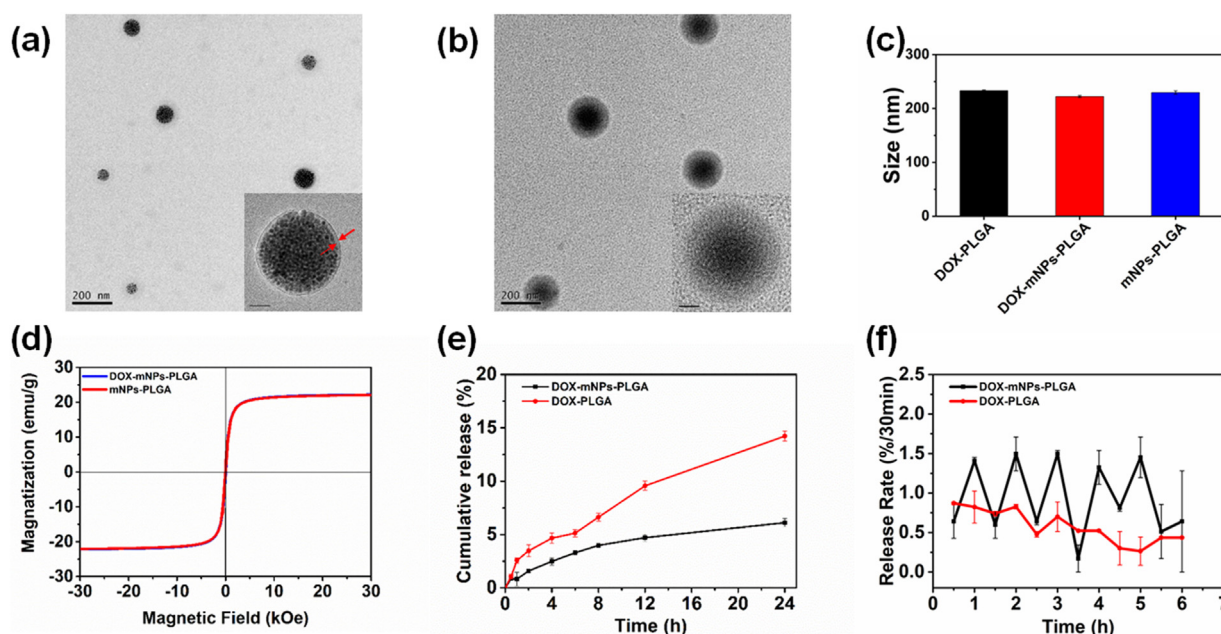

Fig. 2. (a) TEM images of DOX-$Zn_{0.2}Fe_{2.8}O_4$-PLGA nanomaterials. Scale bar is 200 nm. (b) TEM images of DOX-PLGA nanomaterials. Scale bar is 200 nm. (c) Size distributions of DOX-PLGA, $Zn_{0.2}Fe_{2.8}O_4$-PLGA, and DOX-$Zn_{0.2}Fe_{2.8}O_4$-PLGA nanomaterials measured by DLS. (d) Magnetic hysteresis loop of dry DOX-$Zn_{0.2}Fe_{2.8}O_4$-PLGA and $Zn_{0.2}Fe_{2.8}O_4$-PLGA at 300 K by vibrating sample magnetometer (VSM). (e) DOX release profiles of DOX-$Zn_{0.2}Fe_{2.8}O_4$-PLGA and DOX-PLGA nanomaterials within 24 h without RMF. (f) DOX release profiles of DOX-$Zn_{0.2}Fe_{2.8}O_4$-PLGA and DOX-PLGA nanomaterials within 6 h with RMF, initial state of RMF is 'off', the RMF 'on' and 'off' shifts per 30 min.

magnetization (ca. 70 emu/g), and others, were investigated to ensure the consistency of the synthesized nanomaterials and presented in Fig. S1 (Supporting Information, SI). After being thoroughly characterized, the mNPs were encapsulated together with the DOX chemotherapeutic drug in PLGA by the emulsion solvent diffusion evaporation method [19], to form a co-loaded polymerized nanomaterial (DOX-$Zn_{0.2}Fe_{2.8}O_4$-PLGA) with size of ca. 200 nm (Fig. 2a and b). Additionally, DOX-$Zn_{0.2}Fe_{2.8}O_4$-PLGA exhibits similar morphology and hydrodynamic size with the DOX-PLGA and $Zn_{0.2}Fe_{2.8}O_4$-PLGA (Fig. 2c), which we also synthesized for use as control samples. To better understand the resulted material, an array of co-loaded polymerized nanomaterials that were synthesized as dependencies on the payload ratio was systematically analyzed (Table S1). Based on the performed measurements, the following physical parameters were determined: inner structure,

morphology, hydrodynamic size, Zeta-potential, saturation magnetization, and FTIR (Figs. S2 to S5). It is important to mention here that the proposed nanomaterial can be obviously designed to exhibit various payload ratios of its three components, DOX, $Zn_{0.2}Fe_{2.8}O_4$ mNPs, and PLGA. In this regard, we have evaluated three variants which differ in terms of DOX, PLGA, and $Zn_{0.2}Fe_{2.8}O_4$ mNPs quantities/ratios. Various tests described in SI (section II and III), demonstrate the optimal structure among the three variants we experimented with, in terms of the best therapeutic efficiency (cancer cell viability decrease). These tests show that high amounts of the mNPs and DOX are encapsulated in the PLGA due to their electrostatic attractions, which typically results in higher payload ratio and saturation magnetization. When the DOX load increases from 2.75 % to 3.44 %, the drug loading of the mNPs also increases from 0.91 % to 5.64 % (Table S2). Consequently, we can argue

that the DOX-$Zn_{0.2}Fe_{2.8}O_4$-PLGA acts as an excellent material that effectively holds the DOX, representing a reliable drug-carrier. Entrapping drugs in such nanoscale structures is important for enabling next-generation therapies based on mNPs which exhibit the superb capacity to release the entrapped drugs at precise time-points and locations by magnetic triggering. The results of the performed investigations show that the synthesized mNPs and DOX are successfully encapsulated in PLGA with the optimal payload ratio to form the controllable mechano-chemotherapeutic nanomaterial, DOX-$Zn_{0.2}Fe_{2.8}O_4$-PLGA. These features nicely complement the fact that the proposed nanomaterial demonstrates excellent stability (see Fig. S6) and good dispersibility (see Table S3) in physiological conditions, alongside low toxicity owing to the high biocompatibility of PLGA [20]. As the performance of DOX-mNPs-PLGA 3# (Table S1) was found to be the best among the three considered ratios of composites, it was used for further experiments and hereafter referred to as DOX-mNPs-PLGA for simplicity.

Magnetically switchable drug release

The DOX-$Zn_{0.2}Fe_{2.8}O_4$-PLGA incorporates $Zn_{0.2}Fe_{2.8}O_4$ mNPs, which confers it with excellent magnetic responsiveness. The magnetic properties of $Zn_{0.2}Fe_{2.8}O_4$ mNPs were extensively discussed in our previous work, where these mNPs were demonstrated as efficient agents for magnetic resonance imaging [21]. Fig. S7, illustratively presents the magnetic properties of DOX-$Zn_{0.2}Fe_{2.8}O_4$-PLGA: while a magnet is kept close to the aqueous solution, in a short time (~10 s), the nanomaterial rapidly moves toward the magnet, indicating that it can be manipulated by means of an external static magnetic field. In Fig. S8, we show that DOX-$Zn_{0.2}Fe_{2.8}O_4$-PLGA also exhibits a superparamagnetic behavior, with saturation magnetization of 22 emu/g. According to this, a strong magnetic domain of DOX-$Zn_{0.2}Fe_{2.8}O_4$-PLGA was demonstrated by magnetic force microscopy (MFM), as shown in Fig. S9. Such features indicate that this nanomaterial can efficiently be controlled by external magnetic fields, which we exploit for controlled drug release and mechanotherapy. To achieve this, as discussed also in the introduction, we employed a self-designed magnetic equipment (Section IV in SI and illustrated in Fig. S10), capable of generating external magnetic fields whose strength can be precisely tuned. In Fig. S11, after 2 h RMF, we found that DOX-$Zn_{0.2}Fe_{2.8}O_4$-PLGA are arranged in an arc shape and no magnetocaloric effects are produced (see Fig. S12), which indicates that they moved in an arc; this arc-shaped movement will exert an impact force onto the objects the nanomaterials interact with.

As shown in Fig. 2e, DOX-PLGA and DOX-$Zn_{0.2}Fe_{2.8}O_4$-PLGA present drug release profiles characterized by <15 % DOX diffusing out of the nanocarriers within 24 h. The longer cumulative drug release from DOX-$Zn_{0.2}Fe_{2.8}O_4$-PLGA against the control sample (DOX-PLGA) showcases an improved drug release enabled by the magnetic stimulus. This is attributed to the electrostatic attraction between DOX and $Zn_{0.2}Fe_{2.8}O_4$ mNPs, which prevents DOX to diffuse out of the PLGA. Upon magnetic switch, the magnetic energy is transformed into mechanical motive energy, and hence the DOX is released due to the centrifuge force of the mNPs. To investigate the effect of this process in terms of drug release, DOX-$Zn_{0.2}Fe_{2.8}O_4$-PLGA nanomaterials were dispersed in PBS for 30 min, so that the heating effect can be homogenously distributed. As shown in Fig. 2f, at first, the RMF was switched "on" (low strength: 45 m T, rotating speed: 2000 rpm) for 30 min allowing the nanomaterials to move around for subsequent DOX release. Afterwards, the RMF was switched "off" for 30 min allowing the samples to stop the DOX release. Whenever the magnetic field was switched "on" or "off", the drug release rate over the last 30 min was measured. This process was repeated 6 times. The drug release rate of DOX-$Zn_{0.2}Fe_{2.8}O_4$-PLGA was observed to rapidly increase when the

magnetic field was applied, and to dramatically decrease when the applied magnetic field was deactivated. This indicates that the tunable magnetic switch can effectively trigger the drug release from the nanocarrier, thus showcasing one important feature of our proposed novel mechano-chemotherapy. The same experiment was also carried out for DOX-PLGA. In this case, it was observed that the drug release rate of DOX-PLGA naturally decreases irrespective of RMF exposure, owing to the absence of mNPs for DOX "grabbing", thus the release property of the DOX-PLGA cannot be switched on and off.

Magnetomechanical effect for promoting tumour cell death

In the previous section, we discussed the ability of the DOX-$Zn_{0.2}Fe_{2.8}O_4$-PLGA nanomaterial to release the entrapped drug in a controllable manner based on a magnetic switch that can be operated remotely. This ability proposes DOX-$Zn_{0.2}Fe_{2.8}O_4$-PLGA as a solution for chemotherapy, and for other therapies where precise control of the drug release is desired. In this context, we find important to mention that previous studies showed that the cellular uptake of NPs is highly dependent on size, where NPs with small size are normally phagocytized faster than their large analogues [22,23]. To understand how these previous findings correlate with the proposed nanomaterial, we investigated by X-ray fluorescence microscopy MCF-7 cells that were incubated for two different time intervals (8 h and 24 h), together with DOX-$Zn_{0.2}Fe_{2.8}O_4$-PLGA. This investigation modality allowed us to detect the cellular signal corresponding to the Fe element, as shown in Fig. S13 (see section V in SI). The implemented imaging assay shows that DOX-$Zn_{0.2}Fe_{2.8}O_4$-PLGA are not internalized by the cells after 8 h, but are adsorbed by the cells after 24 h of co-incubation. Therefore, to analyze the mechano- and chemotherapeutic effects of the DOX-$Zn_{0.2}Fe_{2.8}O_4$-PLGA upon magnetic induction, the cytotoxicity of MCF-7 and MCF-7/ADR cell lines (the latter a drug-resistant variant of the first, see Fig. S14) were evaluated by an MTT assay only after a co-incubation interval of 24 h.

The cells (density: $1*10^5$) were cultured at physiological conditions for 2 days. Afterwards, DOX-$Zn_{0.2}Fe_{2.8}O_4$-PLGA, DOX-PLGA, and $Zn_{0.2}Fe_{2.8}O_4$-PLGA were separately co-incubated with the two cell lines for 24 h at physiological conditions. Both DOX loaded nanomaterials contained 8 μg/mL of DOX. As shown in Fig. 3a and b, compared with the control (MCF-7 cells only), no significant decrease in the viabilities of cells in the presence of $Zn_{0.2}Fe_{2.8}O_4$-PLGA and DOX-$Zn_{0.2}Fe_{2.8}O_4$-PLGA without RMF is observed (ca. 85 % of cells survived). However, the cell viabilities decrease to about 55 % for the DOX-PLGA groups. This indicates that the DOX-$Zn_{0.2}Fe_{2.8}O_4$-PLGA nanomaterial is in a stable state due to electrostatic attractions occurring between the DOX molecules and the $Zn_{0.2}Fe_{2.8}O_4$ NPs, which result in the non-release of the DOX in the absence of an RMF. Conversely, for DOX-PLGA the cell viabilities decreased to about 55 %, in the absence of RMF (which has no effect due to the lack of magnetic responsiveness of this group). These results correspond to those of *in vitro* drug release studies (Fig. 2f). Furthermore, we observed that by applying an RMF (low strength: 45 m T, rotating frequency: 2000 rpm), the cell viabilities of $Zn_{0.2}Fe_{2.8}O_4$-PLGA and DOX-$Zn_{0.2}Fe_{2.8}O_4$-PLGA groups rapidly decrease, proportionally to the RMF application duration (1 or 2 h), as shown in the heatmap of Fig. 3b. After an RMF exposure interval of 2 h, we observed that the cell viabilities of the DOX-$Zn_{0.2}Fe_{2.8}O_4$-PLGA group not only decrease significantly, but the extent of the decrease is considerably higher compared to the DOX-PLGA group. This indicates that in the case of the DOX-$Zn_{0.2}Fe_{2.8}O_4$-PLGA, besides the chemotherapeutic effect of the released drug, other effects contribute as well to the cell death. We hypothesize that these effects are of mechanical nature, and assume that the magnetomechanical force promotes the death of
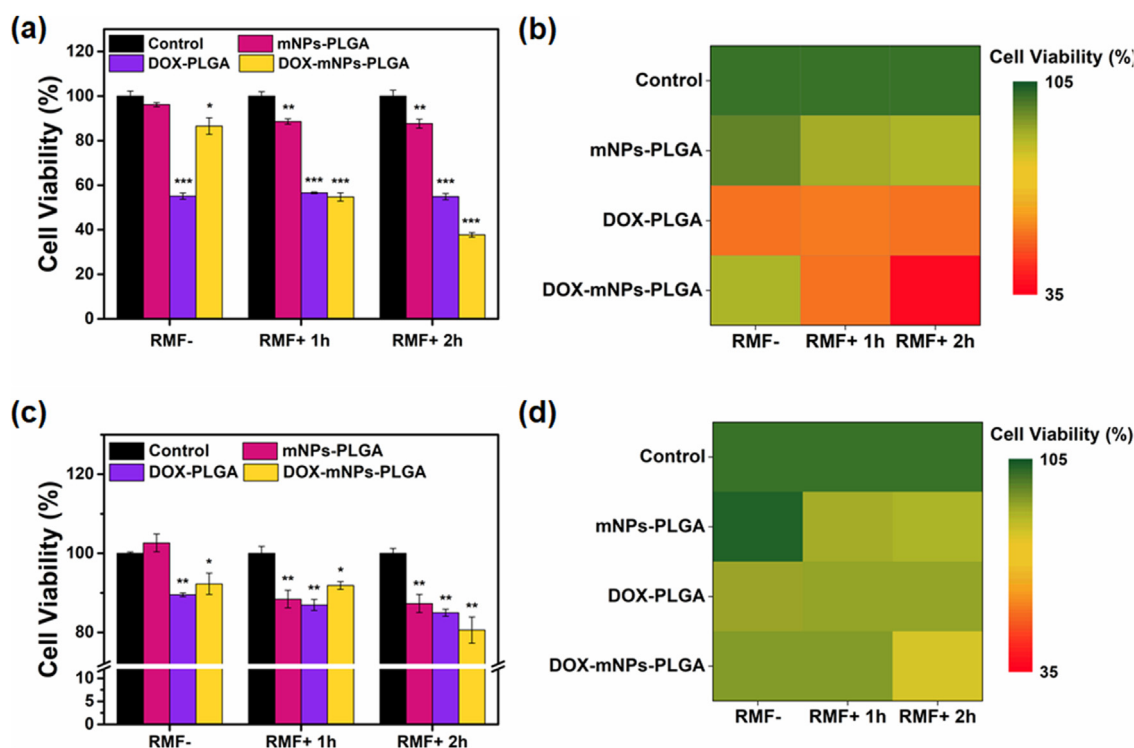
Fig. 3. Cell viability of (a) MCF-7 and (c) MCF-7/ADR cells incubated with $Zn_{0.2}Fe_{2.8}O_4$-PLGA, DOX-$Zn_{0.2}Fe_{2.8}O_4$-PLGA, and DOX-PLGA for 24 h (without RMF), 24 h (with 1 h RMF) and 24 h (with 2 h RMF), respectively. DOX concentrations are 8 μg/mL. (b) and (d) are the color maps of (a) and (c), respectively. *$P < 0.05$, **$P < 0.01$ and ***$P < 0.001$ indicate statistical differences between the two groups shown in the corresponding panels. Data are expressed as mean ± standard deviation. The error bars are based on the results of five experiments per group.

MCF-7 cells. Having thus two effects that results in cell death, magnetomechanical and magneto-chemotherapeutic, explains why the application of DOX-$Zn_{0.2}Fe_{2.8}O_4$-PLGA results in higher amount of "killed" tumour cells, compared to the application of DOX-PLGA.

To verify our hypothesis and understand whether the result that we noticed in the case of DOX-$Zn_{0.2}Fe_{2.8}O_4$-PLGA, namely enhanced tumour cell death, holds indeed also drug-independent reasons, we have repeated the experiment with MCF-7/ADR cells, a drug-resistant variant of MCF-7. As shown in Fig. 3c and d, no significant decreases in cell viabilities can be observed after co-incubating the MCF-7/ADR cells with DOX-PLGA and DOX-$Zn_{0.2}Fe_{2.8}O_4$-PLGA (without RMF) (ca. 90 % of the cells survived), due to the fact that these cells are resistant to DOX. However, upon RMF application, the cell viabilities of $Zn_{0.2}Fe_{2.8}O_4$-PLGA and DOX-$Zn_{0.2}Fe_{2.8}O_4$-PLGA gradually decrease, indicating that the MCF-7/ADR cells are killed by the mechano-therapeutic effect. Therefore, the magnetomechanical force exhibited by the proposed material has the capacity to induce death in drug-resistant cells. Moreover, the magnetomechanical effect highly correlates with the payload ratio of the nanomaterials (see Fig. S15 and S16, and section VI in SI).

To better understand this process, we employed an imaging approach that allowed us to observe the DOX-$Zn_{0.2}Fe_{2.8}O_4$-PLGA nanomaterial inside the cell. As DOX is fluorescent, DOX-PLGA and DOX-$Zn_{0.2}Fe_{2.8}O_4$-PLGA are also fluorescent by virtue of their DOX compositions, as shown in Fig. 4. We used confocal laser scanning microscopy (CLSM), to investigate MCF-7 and MCF-7/ADR cells exposed to both nanomaterials at the same concentration as used in the MTT assay with the magnetic switch in on/off status, respectively. Different cellular structures were labeled by fluorescence staining; nuclei were labeled by Hoechst and cytoskeletons were labeled by fluorescein isothiocyanate (FITC). This labeling strategy allowed us to characterize the geometry and morphology of the cells upon their interactions with the evaluated nanomaterials. As

expected, we observed that the two nanomaterials are sufficiently internalized by both MCF-7 and MCF-7/ADR cells. While the external RMF is turned 'on', the geometry and morphology of the cells co-incubated with DOX-$Zn_{0.2}Fe_{2.8}O_4$-PLGA changed in comparison with those without RMF application. Through quantification of DOX mean fluorescence signal intensity, it can be observed that the fluorescence intensity of DOX in the DOX-mNPs-PLGA group significantly increased after 2 h RMF (see Fig. S17). Furthermore, these results reveal that the fluorescence of the DOX molecules in the co-loaded nanomaterial batch is quenched (due to their electrostatic attractions to the $Zn_{0.2}Fe_{2.8}O_4$ mNPs as a result of electronic energy transfer [24–26]), but comes alive when the external RMF is turned 'on'. These findings correlate with the fluorescence spectra of the corresponding nanomaterials (see Fig. S18 and section VII in SI). In addition, to verify the exact location of the DOX-$Zn_{0.2}Fe_{2.8}O_4$-PLGA agents in a single cell, an X-ray 3D technique was used to identify the signals corresponding to the Fe element. As shown in Fig. 5a and b, some of the DOX-$Zn_{0.2}Fe_{2.8}O_4$-PLGA nanomaterials position near the cell nucleus due to late endosomes/lysosomes which are known to be localized in the area surrounding the nucleus [27,28], while the $Zn_{0.2}Fe_{2.8}O_4$-PLGA nanomaterials are randomly distributed in the plasma of MCF-7 cells after 24 h incubation with/without 2 h RMF induction. However, as shown in Fig. 5c and d, in the case of MCF-7/ADR cells, most DOX-$Zn_{0.2}Fe_{2.8}O_4$-PLGA agents are found to be positioned in the cell membrane and the $Zn_{0.2}Fe_{2.8}O_4$-PLGA agents in the plasma as a result of DOX being extruded out of the MCF-7/ADR cells due to exocytosis of drug-resistant tumour cells [2,29]. In fact, the result of Fig. 5e, which presents the mass of materials in the cells, indicates the polymerized DOX-$Zn_{0.2}Fe_{2.8}O_4$-PLGA can indeed be extruded out of the MCF-7/ADR cells.

To demonstrate the efficiency of the proposed controllable mechano-chemotherapy in terms of "killing" tumour cells, we used a self-designed system capable of yielding tunable RMF. Such tunability is important to investigate how different rotation speeds
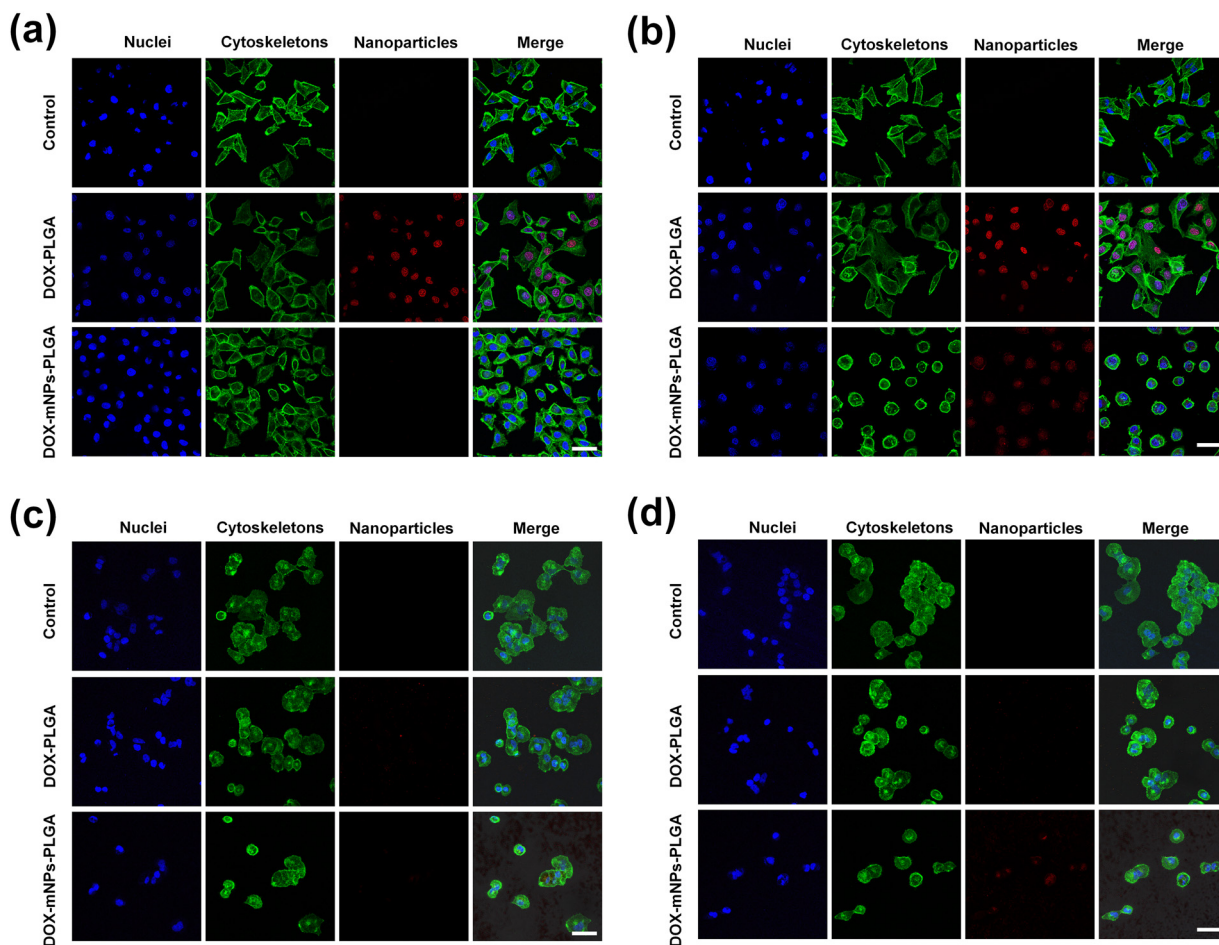
Fig. 4. CLSM images of MCF-7 cells incubated with DOX-PLGA and DOX-$Zn_{0.2}Fe_{2.8}O_4$-PLGA for (a) 24 h (without RMF) and (b) 24 h (with 2 h RMF), respectively. Scale bar is 20 μm. CLSM images of MCF-7/ADR cells incubated with DOX-PLGA and DOX-$Zn_{0.2}Fe_{2.8}O_4$-PLGA for (c) 24 h (without RMF) and (d) 24 h (with 2 h RMF), respectively. Scale bar is 50 μm.
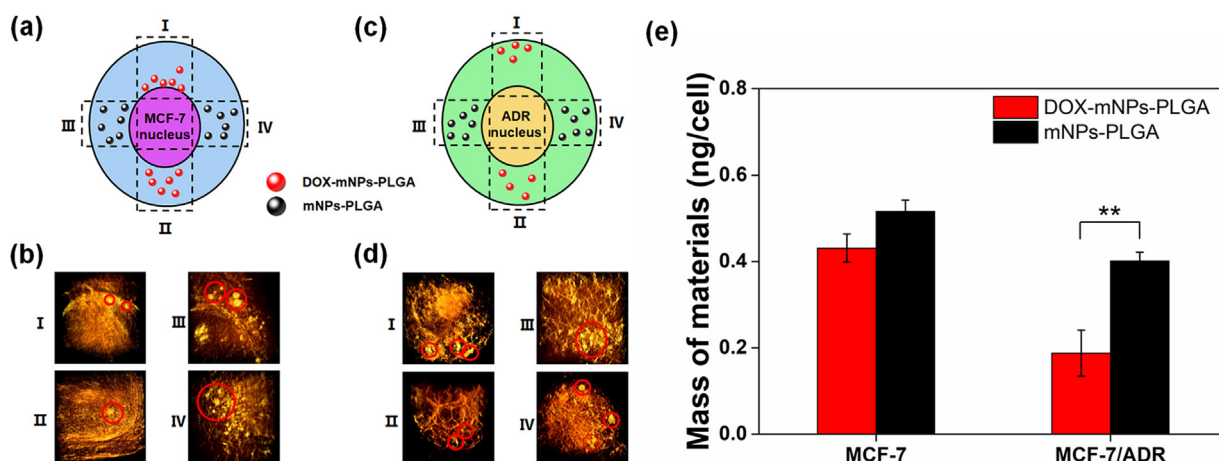

Fig. 5. (a) schematic representation of soft X-ray map of MCF-7 cells after treatment with DOX-$Zn_{0.2}Fe_{2.8}O_4$-PLGA or $Zn_{0.2}Fe_{2.8}O_4$-PLGA nanomaterials for 24 h (without RMF) and 24 h (with 2 h RMF), respectively (I: DOX-$Zn_{0.2}Fe_{2.8}O_4$-PLGA, RMF-; II: DOX-$Zn_{0.2}Fe_{2.8}O_4$-PLGA, RMF+; III: $Zn_{0.2}Fe_{2.8}O_4$-PLGA, RMF-; IV: $Zn_{0.2}Fe_{2.8}O_4$-PLGA, RMF+). (b) Results obtained for cases I—IV in (a), respectively. (c) Scheme of soft X-ray map of MCF-7/ADR cells after treatment with DOX-$Zn_{0.2}Fe_{2.8}O_4$-PLGA or $Zn_{0.2}Fe_{2.8}O_4$-PLGA nanomaterials for 24 h (without RMF) and 24 h (with 2 h RMF), respectively (I: DOX-$Zn_{0.2}Fe_{2.8}O_4$-PLGA, RMF-; II: DOX-$Zn_{0.2}Fe_{2.8}O_4$-PLGA, RMF+; III: $Zn_{0.2}Fe_{2.8}O_4$-PLGA, RMF-; IV: $Zn_{0.2}Fe_{2.8}O_4$-PLGA, RMF+). (d) Results obtained for cases I—IV in (c), respectively. (e) Mass of DOX-$Zn_{0.2}Fe_{2.8}O_4$-PLGA or $Zn_{0.2}Fe_{2.8}O_4$-PLGA engulfed in each cell after incubation for 24 h. **$P < 0.01$ indicate statistical differences between the two groups shown in the corresponding panels. Data are expressed as mean ± standard deviation. The error bars are based on the results of five experiments per group.

and magnetic strengths influence the achieved results (see more details in section VIII of SI). The calculated minimum force under simulated condition that is required to damage the cells is 244.78 pN and the maximum force is 3870.85 pN, because a force in amount of tens of piconewtons can lead to cell death by intracellular pathway and hundreds of piconewtons force can damage
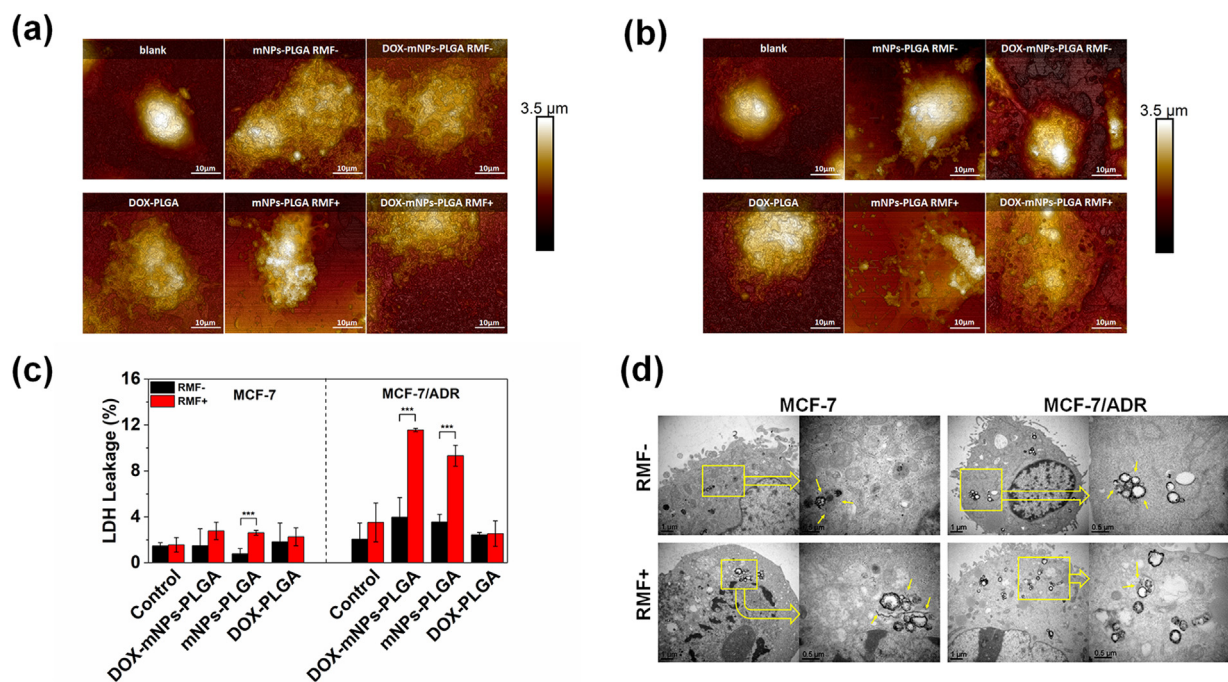
Fig. 6. (a) AFM images of (I) MCF-7 and (II) MCF-7/ADR cells. (b) LDH release from MCF-7 and MCF-7/ADR cells after treatment with DOX-$Zn_{0.2}Fe_{2.8}O_4$-PLGA, $Zn_{0.2}Fe_{2.8}O_4$-PLGA, and DOX-PLGA (DOX: 8 μg/mL, mNPs: 130 μg/mL) without and with RMF for 2 h. (c) Bio-TEM images of $Zn_{0.2}Fe_{2.8}O_4$-PLGA nanomaterials incubated with MCF-7 and MCF-7/ADR cells for 24 h (without RMF) and 24 h (with 2 h RMF), respectively. The yellow arrows point at the lysosomal membranes. ***$P < 0.001$ indicate statistical differences between the two groups shown in the corresponding panels. Data are expressed as mean ± standard deviation. The error bars are based on the results of five experiments per group.

the cell membrane [30,31]. To better understand what happens to the cells when such mechanical forces are applied, we used Atomic Force Microscopy (AFM) to observe the surface and morphology changes of the MCF-7 and MCF-7/ADR cells incubated with all three nanomaterials (DOX-$Zn_{0.2}Fe_{2.8}O_4$-PLGA, DOX-PLGA, and $Zn_{0.2}Fe_{2.8}O_4$-PLGA), for the case where an RMF (low strength: 45 m T, rotating frequency: 2000 rpm) was applied for 2 h, in Fig. 6a and b. Significant depressed deformations were observed on the surfaces of the MCF-7 and MCF-7/ADR cells incubated with $Zn_{0.2}Fe_{2.8}O_4$-PLGA and DOX-$Zn_{0.2}Fe_{2.8}O_4$PLGA, in the presence of an active RMF. This observation suggests that cell membranes of MCF-7 and MCF-7/ADR can be ruptured by the magnetomechanical force, which corresponds to the experimental results of lactate dehydrogenase (LDH) in Fig. 6c. As shown in Fig. 6d, the physical treatment using magnetomechanical force leads to leakage of lysosome hydrolases into the cytosol, which induces programmed cell death by apoptosis. Considering that DOX can also induce apoptosis [32,33], our results indicate that the proposed DOX-$Zn_{0.2}Fe_{2.8}O_4$-PLGA nanomaterial efficiently induces cell apoptosis as a result of a combined effect of magnetomechanical force exerted on the cell and chemotherapy, supposing a low magnetic field (45 m T) is applied.

To summarize this section, based on the results described above, we argue that the proposed magnetomechanical effect represents a viable solution for promoting death in drug-resistant cells, which cannot be eliminated using conventional treatment approaches based on chemotherapy. The magnetomechanical force has the ability to kill drug-resistant tumor cells by damaging their cell membranes. Also important, in tumor cells that are not drug-resistant, the two complementary therapeutic routes, namely chemotherapy and mechanotherapy, result in higher efficiency compared to using solely the former one. Therefore, the most important finding of our work is that the developed material, DOX-$Zn_{0.2}Fe_{2.8}O_4$-PLGA, is very efficient at destroying tumor cells irrespective of whether they are drug-resistant or not.

Biosafety of DOX-$Zn_{0.2}Fe_{2.8}O_4$-PLGA agents in vivo

To further investigate the suitability of the proposed DOX-$Zn_{0.2}Fe_{2.8}O_4$-PLGA nanomaterial as a therapeutic agent, we turned our attention towards assessing its toxicity in an *in vivo* mouse model. For this purpose, 100 μL of DOX-$Zn_{0.2}Fe_{2.8}O_4$-PLGA nanomaterial was intravenously injected into mice via the tail veins. According to the blood circulation system, the nanomaterials are prone to be transported to the main organs of the mice, including heart, liver, spleen, lung and kidney. Inductively coupled plasma mass spectrometry (ICP-MS) was used for measuring the Fe element in order to quantitatively estimate the contents of the proposed nanomaterials in these organs, which is important for assessing their *in vivo* toxicities. As shown in Fig. 7a, after injection, the concentration of Fe significantly increased in the spleen and liver compared to the other organs, owing to the high accumulation of DOX-$Zn_{0.2}Fe_{2.8}O_4$-PLGA by the immune system. However, after 12 h, the Fe concentration dramatically decreased in the liver but increased in the other organs, indicating good biocompatibility and circulation *in vivo*. Additionally, an increase of the Fe concentration was observed in kidneys after 12 h, but this decreased after 24 h, indicating good biodegradability. Fe (and hence the proposed DOX-$Zn_{0.2}Fe_{2.8}O_4$-PLGA) were barely found in the brain, as a result of the blood brain barrier.

To further evaluate the toxicity, the major organs of the mammalian body were subjected to histological assessment, which was conducted to see whether the injected nanomaterial induced any tissue damage, inflammation or lesions. This examination was implemented on the 14th day post-injection. As shown in Fig. 7b, the pathological assessment of the main organs after injection of DOX-$Zn_{0.2}Fe_{2.8}O_4$-PLGA, $Zn_{0.2}Fe_{2.8}O_4$-PLGA, and DOX-PLGA demonstrated that no damage was inflicted to the heart, liver, spleen, lung, and kidney. These results indicate thus that the proposed mechano-chemotherapeutic nanomaterial exhibits good biocompatibility and biodegradability at the tested concentration,
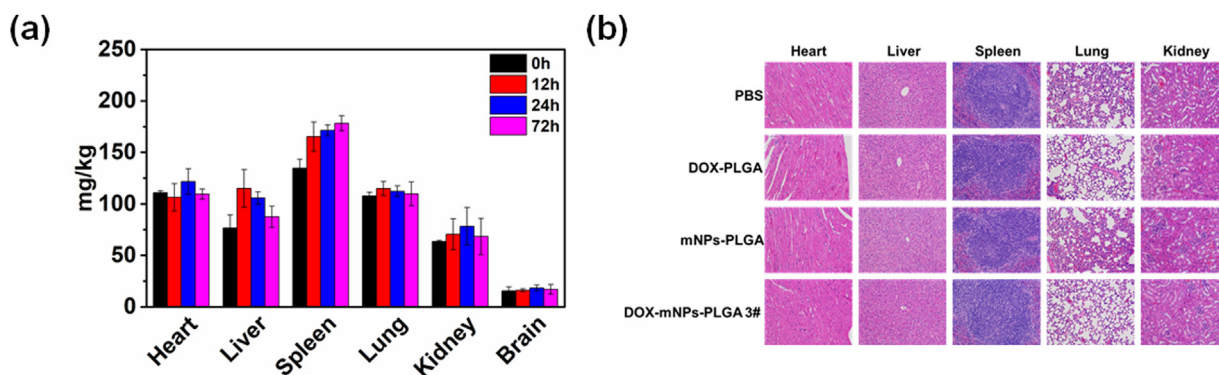
Fig. 7. (a) Biodistribution of the Fe element in major mice organs at 0, 12, 24, and 72 h post-injection intravenously. (b) H&E staining images of the major organs collected from mice after different treatments on the 14th day (scale bar: 100 μm).

which promotes it as a solution worthy to consider. However, if other future applications will come to require the use of these nanomaterials in larger doses, additional studies will be required to investigate systematically, and in detail, the corresponding biological safety aspects.

Conclusion

In this work, we have developed a novel therapeutic method termed mechano-chemotherapy, and demonstrated it using a controllable mechano-chemotherapeutic nanomaterial, which was constructed by co-loading $Zn_{0.2}Fe_{2.8}O_4$ mNPs and the DOX anticancer drug into a PLGA shell. The so-achieved nanomaterial can be easily controlled by an external magnetic field as a result of its superb magnetic response, and is highly stable in physiological environment due to the ultra-high biocompatibility of the PLGA shell. The proposed agent, DOX-$Zn_{0.2}Fe_{2.8}O_4$-PLGA, has a dual functionality. First, the entrapped drug can be controllably released by using a magnetic switch, based on a tunable RMF equipment (45 m T and 2000 rpm in this work). This allows safe and efficient chemotherapy to be realized in a precise, non-invasive and remote manner. Second, the $Zn_{0.2}Fe_{2.8}O_4$ mNPs entrapped in the proposed material, under the influence of an external RMF generate a mechanical force that inflicts significant damage to tumour cells, resulting in their death. Thus, the proposed nanomaterial possesses the capacity to induce tumour cell death by two distinct and complementary mechanisms, with the big advantage that it can address both drug-resistant and typical tumor cells. The proposed material was demonstrated to be non-toxic, in an *in-vivo* mouse model, which suggests that it can be safely applied in mammals. Based on the obtained results, we believe that the proposed material has great potential for enhancing current therapeutic approaches. Furthermore, given the MRI contrast of $Zn_{0.2}Fe_{2.8}O_4$, the proposed DOX-$Zn_{0.2}Fe_{2.8}O_4$-PLGA therapeutical agent can also be exploited for imaging, which would allow activating its tumor destructive properties once its position at the exact pathological site is confirmed (by MRI), in potential high-precision theranostic applications. Last but not least, the concept behind this material, can be used in association with other drugs, and other magnetic materials, thus it can be useful in addressing a wide range of pathologies affecting various organs.

Materials and methods

Materials and reagents

Ammonium iron (II) sulfate hexahydrate ($FeSO_4 \cdot (NH_4)_2SO_4 \cdot 6H_2O$) and zinc sulfate heptahydrate ($ZnSO_4 \cdot 7$

H_2O) were obtained from Sinopharm Chemical Reagent Co. Ltd (Shanghai, China). Sodium hydroxide (NaOH) and oleic acid (OA) were purchased from Aladdin Industrial Corporation (Shanghai, China). Poly (D,L-lactide-co-glycolide) (PLGA 50:50, Resomer RG 503, MW: 24000−38000 Da), polyvinyl alcohol (PVA, Mowiol 4–88), doxorubicin hydrochloride (DOX), phalloidin-FITC, and Hoechst 33,258 were purchased from Sigma-Aldrich (USA). Dulbecco's modified eagle's medium (DMEM), trypsin-EDTA, penicillin–streptomycin, and fetal bovine serum (FBS) were purchased from Gibco-BRL (Grand Island, New York). 3-(4,5-Dimethylthiazol-2-yl)-2,5-diphenyltetrazolium bromide (MTT) was purchased from Merck (Germany). Milli-Q water with a resistivity of 18.2 MΩ cm^{-1} was used in all the experiments. All other chemicals and solvents were of analytical grade and used directly without further purification.

Synthesis of the mNPs

The magnetic zinc-doped iron oxide NPs with average size of 7 nm were prepared according to a previously reported protocol [21], which is modified from a simple and low-cost method based on an OA/alcohol/water system. Briefly, 1.73×10^{-3} mol Fe^{2+} and 1.34×10^{-4} mol Zn^{2+} precursors in 20 mL of Milli-Q water were obtained from ammonium iron (II) sulfate hexahydrate ($FeSO_4 \cdot (NH_4)_2SO_4 \cdot 6H_2O$) and zinc sulfate heptahydrate ($ZnSO_4 \cdot 7H_2O$), respectively. Then, 10 mL of OA, 1 g of NaOH and 10 mL of ethanol were mixed at room temperature via magnetic stirring to obtain a uniform solution. Next, the Fe^{2+} precursor was added to the mixture and the precipitate turned brown under stirring for several minutes. After this, the reactants were transferred to a reaction kettle, which was sealed and heated at 230 °C for 15 h. When the reaction was over, the system was allowed to cool down to room temperature. The black product settled at the bottom of the vessel, and cyclohexane was added to collect the NPs. For the purpose of purifying the NPs, ethanol was added for washing purposes for a few times and the black powder precipitate could be recovered by centrifugation (8000 rpm, 8 min). Finally, the precipitate was dispersed in chloroform, and characterized using transmission electron microscope (TEM) and X-ray diffraction (XRD) spectroscopy.

Synthesis of the polymerized nanomaterials

Co-loaded PLGA NPs were prepared based on the method of emulsion solvent diffusion evaporation [19,34]. Namely, 20 mg PLGA (100 mg/mL) and 1 mg DOX (1.0 mg/mL) were mixed in chloroform ($CHCl_3$) containing zinc-doped iron oxide NPs (7 mg/mL). Then, the mixture was added dropwise into 1 % PVA aqueous solu-

tion under an ice bath and the sonifier was set at 35 % power. After sealed stirring for 30 min, the homogeneous emulsion was kept stirring overnight and was allowed to evaporate ethyl acetate at room temperature. In the end, co-loaded PLGA nanomaterials were gathered using a centrifuge (D-37520, Thermo Electron LED GmbH, Germany) at 10,000 g for 30 min and redispersed in Milli-Q water. The final dispersion was stored at 4 °C for further use. The DOX-PLGA and $Zn_{0.2}Fe_{2.8}O_4$-PLGA were synthesized by the same scheme without zinc-doped iron oxide NPs or DOX, respectively.

Test of encapsulation efficiency and drug loading of DOX and mNPs in nanomaterials

First, a standard curve of DOX was constructed by measuring the absorbance at 480 nm of various concentrations of DOX solution using a UV–vis spectrophotometer (Lambda 950, Perkin Elmer, USA). For preparation of the DOX solution, 10 mg were dissolved in 10 mL water as stock solution. For recording a calibration curve, 1.0 mg/mL DOX solution was diluted into a serial concentration of 0, 0.005, 0.010, 0.015, 0.020, 0.025, 0.030, 0.040, and 0.050 mg/mL. The measurement was performed in quartz cuvettes.

To calculate the encapsulation efficiency (%EE), the supernatant was collected. DOX' concentration in the supernatant was then determined by the ultraviolet absorption at the wavelength of 480 nm, a strong absorption peak of DOX in reference to the constructed calibration curve on a UV–vis Spectrophotometer. Following this step, the encapsulation efficiency (%EE) was obtained.

For drug-loading content, the dried powder of the NPs was dissolved in water-acetonitrile (7:3) solution and shook for 60 s. The DOX concentration in the resulted solution was then determined by UV–vis measurement, and the total amount of the drug in the co-loaded nanomaterial could be calculated. At last, %EE and %drug loading were calculated using Eqs. (1) and (2), respectively:

$$\%EE = \frac{\text{mass of DOX (or Zn0.2Fe2.8O4) in nanomicelles}}{\text{total mass of DOX (or Zn0.2Fe2.8O4)}} \times 100\% \quad (1)$$

$$\%\,\text{Drug loading} = \frac{\text{mass of DOX (or Zn0.2Fe2.8O4) in nanomicelles}}{\text{mass of DOX (or Zn0.2Fe2.8O4) in nanomicelles} + \text{mass of the polymeric material used}} \times 100\% (2)$$

The entrapment efficiency and loading of $Zn_{0.2}Fe_{2.8}O_4$ NPs in PLGA was analyzed by inductively coupled plasma optical emission spectrometry (ICP-OES) using an Optima 2100DV instrument (Perkin Elmer, USA). Briefly, a dispersion of co-loaded nanomaterials was digested with 5 mL HNO_3, 0.5 mL $HClO_4$, and 0.5 mL H_2O_2 in a reaction kettle for about 4 h at 180°C. After that, the sample was diluted with Milli-Q water and the Fe element was measured by ICP-OES. In the end, the %EE and % drug loading could also be calculated using Eqs (1) and (2), respectively.

Morphology and structural characterization

After the preparation of the $Zn_{0.2}Fe_{2.8}O_4$ NPs, DOX-PLGA, $Zn_{0.2}Fe_{2.8}O_4$-PLGA and DOX-$Zn_{0.2}Fe_{2.8}O_4$-PLGA, a series of characterization sessions were carried out. Scanning electron microscopy (SEM) and Transmission electron microscopy (TEM) of DOX-PLGA, $Zn_{0.2}Fe_{2.8}O_4$-PLGA and DOX-$Zn_{0.2}Fe_{2.8}O_4$-PLGA were used to describe the detailed morphological and structural information. SEM images were recorded on a S4800 (Hitachi, Japan) instrument which was operated at 8 kV. TEM images were obtained from a JEOL-2100 (JEOL Ltd, Japan) instrument which was operated at 200 kV. The hydrodynamic size, size distribution (polydispersity, PDI), and Zeta potential of DOX-PLGA, $Zn_{0.2}Fe_{2.8}O_4$-PLGA and DOX-$Zn_{0.2}Fe_{2.8}O_4$-PLGA were measured in Milli-Q water by dynamic light scattering (DLS) using a Zeta particle size analyzer (Nano-ZS, Malvern, England). The mean values were calculated from the measurements performed at least in triplicates. The crystalline phase

of $Zn_{0.2}Fe_{2.8}O_4$ NPs was examined by X-ray diffraction (XRD) measurement on AXS D8 Focus Powers X-ray diffraction diffractometer (Bruker Co., USA) with Cu Kα radiation (λ=0.154 nm).

Magnetic Force Microscopy (MFM) characterization

A Dimension Fast scan Atomic Force Microscope (Bruker Co., USA) was utilized for determining the magnetic domains of the investigated samples at room temperature. All images were obtained in Magnetic Force Microscopy mode, where the magnetic domain was recorded by interaction between a magnetized tip and the sample. A magnetized cobalt-chromium tip (MESP, f_0 = 75 kHz, k = 2.8 Nm^{-1}) with measured resonance frequency of 77.6 kHz and spring constant of 2.57 Nm^{-1} was used for the measurements. The samples were dropped on a mica patch and air-dried for easily inflicting phase separation, so that the magnetic domain being determined to be distinguishable from the mica surface by presenting phase contrast. The magnetic domain reflected in the phase channel clearly presented the magnetic profiles of the samples which were attributed to the loading of the mNPs.

Drug release without RMF in vitro

PBS solution (pH = 7.4) was used as the sustained release medium. Samples (DOX-PLGA and DOX-$Zn_{0.2}Fe_{2.8}O_4$-PLGA) containing 366 μg DOX were mixed with 2 mL PBS solution, then loaded in a dialysis bag with a MWCO of 3500 Da and placed into a centrifuge tube with 8 mL PBS at 37 °C. For measuring the cumulative release of DOX, 2 mL of solution was extracted at specific time points and replaced with the same volume of fresh PBS to maintain sink condition. The absorbance was measured at 480 nm using a UV–vis spectrophotometer.

Drug release with RMF in vitro

Similarly, the DOX-PLGA and DOX-$Zn_{0.2}Fe_{2.8}O_4$-PLGA nanomaterials containing 366 μg DOX were mixed with 2 mL PBS solution, then loaded in a dialysis bag with a MWCO of 3500 Da and placed in a centrifuge tube with 8 mL PBS at 37 °C. The 'on' and 'off' of RMF was controlled by the magnetic stirrer with the interval of 30 min. For measuring the release of DOX at the interval of 30 min, 2 mL solutions were extracted every 30 min and same volume of fresh PBS was added to maintain the sink condition. The absorbance was measured at 480 nm using UV–vis spectrophotometer.

Cell culture

Human breast cancer cell lines (MCF-7) were cultured in a DMEM medium supplemented with 10 % of fetal bovine serum (FBS), 100 unit/mL of penicillin and 100 mg/mL of streptomycin and incubated at 37 °C under a humidified atmosphere of 5 % CO_2. MCF-7/ADR cells were cultured same as MCF-7, but in addition 1 μg/mL DOX was added to ensure drug-resistance. When the cells were grown to 80 %–90 % confluence, these cells were digested, collected and seeded into more cell culture flasks or cell 96-well plates for different assays. All cell lines involved in this experiment

have been obtained from the Cell Bank of the Chinese Academy of Sciences (Shanghai, China).

Cytotoxicity test

The MTT assay was used to evaluate the cytotoxicity of the different mNPs concentrations, and different DOX concentrations of free DOX, DOX-PLGA, and DOX-$Zn_{0.2}Fe_{2.8}O_4$-PLGA. Briefly, 100 μL of 10^5/mL MCF-7 cells were seeded in 96-well plates and cultured at 37 °C, 5% CO_2 for 24 h. Then, the old medium in each well was replaced with 100 μL of fresh medium containing mNPs at 2.5, 25, 50, 100, and 200 μg/mL, and incubated for 24 h. Afterwards, 10 μL (5 mg/mL) of MTT solution was added to each well and further incubated for 4 h. The liquid in each well was aspirated, and 150 μL of dimethyl sulfoxide (DMSO) was added instead. The plate was read at 550 nm (O.D.) with the plate reader and cell viability was calculated. The cytotoxicities of free DOX, DOX-PLGA, and DOX-$Zn_{0.2}Fe_{2.8}O_4$-PLGA were evaluated in a similar manner.

Cell viability experiment under RMF

The MTT assay was also used to assess the cell viability of DOX-PLGA and DOX-$Zn_{0.2}Fe_{2.8}O_4$-PLGA (with payload gradient) under RMF. Briefly, 100 μL of 10^6/mL MCF-7 or MCF-7/ADR cells was seeded in 96-well plates and cultured at 37 °C, 5% CO_2 for 24 h. Afterwards, the medium in each well was replaced with 100 μL of fresh medium containing DOX-PLGA and DOX-$Zn_{0.2}Fe_{2.8}O_4$-PLGA (with payload gradient). The DOX concentration remained consistent at 8 μg/mL, and the cells were co-incubated with the nanomaterials for 22 h. The cell media were discarded and cells were washed with fresh PBS solution for three times to remove materials that were not taken up by the cells, and fresh media were added. The 96-well plate was placed in RMF at 37 °C for 1 and 2 h (2000 rpm, 45 m T) to ensure that total cell incubation time was 24 h. After 2 h of RMF exposure, 10 μL (5 mg/mL) of MTT solution was added to each well and further incubated for 4 h. The liquid in each well was aspirated, and 150 μL of DMSO was added instead. The plate was read at 550 nm (O.D.) with the plate reader and cell viability was calculated.

Confocal laser scanning microscopy (CLSM)

The uptake of DOX-PLGA and co-loaded PLGA nanomaterials by MCF-7 cells was investigated by CLSM. First, 2.0 mL of the MCF-7 cells in DMEM medium were seeded in dishes with the size of ø35 mm at a density of 5.0×10^4 cells per mL and allowed to adhere at 37 °C under a 5 % CO_2 atmosphere overnight. Then the DMEM medium was replaced with a fresh medium containing DOX-PLGA and co-loaded PLGA nanomaterials separately (DOX: 8 μg/mL). After incubation for 8 h, the cells were washed with PBS at least three times, and then covered with 1 mL of 4% paraformaldehyde for 30 min at 4 °C, and permeabilized with 1 mL of 0.1 % triton-100 for 5 min. Next, cells were blocked with 1 mL of 1.0 % BSA for 30 min and then stained with100 μL of Hoechst (5 μg/mL) and FITC (2.5 μg/mL) mixture for 30 min at room temperature. At last, the Hoechst label attached to the nuclei was excited at 405 nm and its emission in the range of 415–480 was collected by a CLSM (TCS SP5 II, Leica, Germany). Similarly, the DOX was excited at 488 nm and its emission was collected in the range of 515−540 nm. The FITC label attached to the cell membrane was excited at 543 nm and the observed emission range was 600−720 nm.

LDH release assays

The LDH release from MCF-7 and MCF-7/ADR cells incubated with DOX-PLGA, $Zn_{0.2}Fe_{2.8}O_4$-PLGA, and DOX-$Zn_{0.2}Fe_{2.8}O_4$-PLGA for 24 h with/out RMF was analyzed. The absorption intensities at 450 nm of cell culture media containing LDH test working solution were measured, and the LDH leakage was calculated as LDH leakage (%) = [(absorbance of treatment cells − absorbance of control cells)/(absorbance of maximal enzyme activity cells − absorbance of control cells)] × 100. The assays were conducted according to the corresponding user instructions provided by the kit manufacturers.

AFM characterization of cell membrane morphology

All AFM characterizations of the morphology of the cell membranes were performed at room temperature in liquid phase. All figures were obtained with a Bioresolve AFM (Bruker. Co., USA) in ScanAsyst mode. The cell samples were incubated on a coverslip and then transferred into PBS for measurement. A ScanAsyst probe (SCANASYST-FLUID, f_0 = 150 kHz, k = 0.7 Nm^{-1}) was used for measurements and the applied force on the cells was minimized (optimized). The morphologies and surface changes of the cells were monitored, and all figures were analyzed using the Nanoscope Analysis software (Bruker Co., USA). All information available in the height channel clearly reflects the morphological profiles and surface changes of the cells (which resulted from their interaction with the evaluated nanomaterials).

X-ray fluorescence imaging (XFM)

The cellular uptake of mNPs by MCF-7 cells was investigated by X-ray fluorescence microscopy at the Shanghai Synchrotron Radiation Source Hard X-rays BL15U1 Beamline Nano Station of China. Simply, 1 mL of 20,000/mL MCF-7 cells were seeded in 24-well plates and cultured at 37 °C, 5 % CO_2 for 24 h. Afterwards, 1 mL of the old medium in each well was replaced with fresh medium containing DOX-$Zn_{0.2}Fe_{2.8}O_4$-PLGA with DOX concentration of 8 μg/mL, and incubated for 8 h (8 h without RMF, 6 h without RMF +2 h RMF) and 24 h (24 h without RMF, 22 h without RMF +2 h RMF). Following RMF, the cells were washed with PBS at least three times, and then covered with 1 mL of 4% paraformaldehyde for 30 min at 4 °C. Finally, 1 mL of PBS was added to prevent the cells from drying. Hard X-ray energy was 10 keV, collecting Fe, S, and Cl elements when imaging the MCF-7 cells.

Soft X-ray 3D imaging

The X-ray Nano-CT experiment was performed with a BL07W beamline at the National Synchrotron Radiation Laboratory (NSRL) in Hefei of China. The X-rays were focused by an elliptical capillary condenser. In combination with a microzone plate, the whole system can perform absorption imaging with X-ray energies ranging from 280 to 700 eV and a spatial resolution of 30 nm. Typically, MCF-7 or MCF-7/ADR cells are seeded in 100-mesh TEM nickel grids. After cells adhered to the walls, the old medium in each well was replaced with fresh medium containing $Zn_{0.2}Fe_{2.8}O_4$-PLGA or DOX-$Zn_{0.2}Fe_{2.8}O_4$-PLGA with Fe concentration of 100 μg/mL, and incubated for 24 h (24 h without RMF, 22 h without RMF +2 h RMF). Grids with cell samples were moved in the homemade freezer plunge and rapidly put into the liquid nitrogen in the cryopreserving container to freeze the cells at liquid nitrogen temperature. Then, the grids with cell samples were transferred to the soft X-ray imaging vacuum cryogenic chamber. In this experiment, a X-ray energy of 520 eV was applied for cell imaging. The exposure time for each projection image was 300 ms. Following this step, we applied the total variation based simultaneous algebraic reconstruction technique as an iterative reconstruction method to further assess the subcellular structure information in 3D space [35]. By rotating the specimen on the sample stage, 121 cell projection images were collected in the 10 μm field of view with a tilting angle of 1°

from –60° to 60° for monographic reconstruction. After recording the automatic projections, the projection image stack was manually aligned with the open source software IMOD by tracking the marker points from specific features of the specimen cell. The marker points were taken as the aligning fiducial makers on the neighboring images in the stack. Cross-section slice images of the specimen cell in 3D could then be obtained from the reconstruction.

Characterization of cellular uptake of nanomaterials by Bio-TEM

The Bio-TEM imaging sessions conducted to assess the cellular uptake of nanomaterials were performed at the Bio-ultrastructure Analysis Laboratory of the Analysis Center of Agrobiology and Environmental Sciences, Zhejiang University, China. Briefly, 1 mL of 50,000/mL MCF-7 cells and MCF-7/ADR cells were seeded in 24-well plates and cultured at 37 °C, 5 % CO_2 for 24 h. In the next step, the old medium in each well was replaced with fresh medium containing $Zn_{0.2}Fe_{2.8}O_4$-PLGA or DOX-$Zn_{0.2}Fe_{2.8}O_4$-PLGA with Fe concentration of 100 µg/mL, and incubated for 24 h (24 h without RMF, 22 h without RMF +2 h RMF). After RMF, the cells were washed with PBS at least three times, and then digested with trypsin, centrifuged for precipitation, and covered with 1 mL of 2.5 % glutaraldehyde for 12 h at 4 °C. Afterwards, the cells were fixed with 1% citric acid solution. The samples were then dehydrated with a gradient of ethanol solution (30 %, 50 %, 70 %, 80 %, 90 %, 95 %, and 100 %). In the final step, the samples were infiltrated, embedded, sliced, stained, and observed under TEM (Hitachi H-7650, Japan).

Mass of materials in single cell

The same number of cells (MCF-7 or MCF-7/ADR) was seeded in a 6-well plate, and DOX-$Zn_{0.2}Fe_{2.8}O_4$-PLGA or $Zn_{0.2}Fe_{2.8}O_4$-PLGA was added and incubated for 24 h after the cells were attached [36]. Then, the number of cells in the blank group was calculated. At the same time, the experimental group was washed with PBS solution for three times, and each well was immersed with 2 mL of aqua regia for 24 h. Finally, the concentration of the Fe element was calculated by ICP-OES. The Mass of materials per cell was calculated as [(mass of $Zn_{0.2}Fe_{2.8}O_4$/%drug loading)/(Number of cells in the blank group*corresponding cell viability)] × 100 %.

Animal models and in vivo toxicity

Female BALB/c mice (4–6 weeks old) were purchased from Nanjing Cavins Biotechnology Co., Ltd (Nanjing, China) and used under protocols approved by the Regional Ethics Committee for Animal Experiments at Ningbo University, China (Permit No. SYXK (Zhe) 2019−0005). For in vivo toxicity, healthy female BALB/c mice were intravenously injected with 150 µL of PBS solution (control group) and 150 µL DOX-PLGA, DOX-$Zn_{0.2}Fe_{2.8}O_4$-PLGA and $Zn_{0.2}Fe_{2.8}O_4$-PLGA distributed in PBS (DOX concentration: 8 µg/mL). After 14 days, the two groups of mice were sacrificed and their major organs (heart, liver, spleen, lung and kidney) were subjected to the Haematoxylin and Eosin (H&E) staining and histopathological assessment.

In vivo biodistribution

Healthy female BALB/c mice were intravenously injected with 150 µL DOX-$Zn_{0.2}Fe_{2.8}O_4$-PLGA distributed in PBS (DOX concentration: 8 µg/mL). After different time intervals since the injection (12, 24 and 72 h), the mice were sacrificed and the obtained-main organs (heart, liver, spleen, lung, kidney and brain) were put into 50 mL centrifuge tubes, and then 2 mL of HNO_3 and 6 mL of HCl were mixed with the above tubes at the water bath (100 °C) for 12 h. When the temperature of the solution was cooled to about 25 °C, it was filtered with a 0.22 µm membrane, then the volume

of solution was increased up to 10 mL by adding pure water. The content of Fe from various organs collected from mice sacrificed at different time intervals since the injection was measured on Inductively Coupled Plasma Optical Emission Spectrometer (ICP-OES, PE Optima 2100DV, Perkin Elmer, USA).

Author statement

F.Y. and A.W. designed the study. Under supervision by F.Y. and A.W., C.Y. and L.S. performed polymerized NPs preparation and Characterization. Y.M. produced magnetic NPs. S.G.S., Z.L., C.L. and O.U.A. developed cell experiments and analysis. L.X. performed the theoretical calculation. F.Y., N.H. and H.L. collected and analysed experimental data. C.Y. and F.Y. wrote the paper. All authors disscussed the results and contributed to the manuscript.

Declaration of Competing Interest

The authors report no competing interests.

Acknowledgements

Appendix A. Supplementary data

Supplementary material related to this article can be found, in the online version, at doi:https://doi.org/10.1016/j.nantod.2020.100967.

References

[1] B.A. Chabner, T.G. Roberts Jr., Nat. Rev. Cancer 5 (2005) 65.
[2] G. Szakacs, J.K. Paterson, J.A. Ludwig, C. Booth-Genthe, M.M. Gottesman, Nat. Rev. Drug Discov. 5 (2006) 219–234.
[3] J.A. Moscow, K.H. Cowan, B.I. Sikic, Holland-Frei Cancer Medicine (2016) 1–7.
[4] S.-h. Noh, S.H. Moon, T.-H. Shin, Y. Lim, J. Cheon, Nano Today 13 (2017) 61–76.
[5] D.-H. Kim, E.A. Rozhkova, I.V. Ulasov, S.D. Bader, T. Rajh, M.S. Lesniak, V. Novosad, Nat. Mater. 9 (2010) 165.
[6] Y. Chen, P. Han, Y. Wu, Z.F. Zhang, Y. Yue, W.H. Li, M.Q. Chu, Small 14 (2018) 13.
[7] Y. Shen, C. Wu, T.Q.P. Uyeda, G.R. Plaza, B. Liu, Y. Han, M.S. Lesniak, Y. Cheng, Theranostics 7 (2017) 1735–1748.
[8] D.H. Kim, E.A. Rozhkova, I.V. Ulasov, S.D. Bader, T. Rajh, M.S. Lesniak, V. Novosad, Nat. Mater. 9 (2010) 165–171.
[9] M.H. Cho, E.J. Lee, M. Son, J.H. Lee, D. Yoo, J.W. Kim, S.W. Park, J.S. Shin, J. Cheon, Nat. Mater. 11 (2012) 1038–1043.
[10] C. Park, K. Oh, S.C. Lee, C. Kim, Angew. Chem.-Int. Edit. 46 (2007) 1455–1457.
[11] T.D. Nguyen, H.R. Tseng, P.C. Celestre, A.H. Flood, Y. Liu, J.F. Stoddart, J.I. Zink, Proc. Natl. Acad. Sci. U.S.A. 102 (2005) 10029–10034.
[12] M.K. Yu, Y.Y. Jeong, J. Park, S. Park, J.W. Kim, J.J. Min, K. Kim, S. Jon, Angew. Chem.-Int. Edit. 47 (2008) 5362–5365.
[13] Z.L. Wang, X.D. Xue, Y.X. He, Z.W. Lu, B. Jia, H. Wu, Y. Yuan, Y. Huang, H. Wang, H.W. Lu, K.S. Lam, T.Y. Lin, Y.P. Li, Adv. Funct. Mater. 28 (2018) 12.
[14] H.L. Xu, K.L. Mao, Y.P. Huang, J.J. Yang, J. Xu, P.P. Chen, Z.L. Fan, S. Zou, Z.Z. Gao, J.Y. Yin, J. Xiao, C.T. Lu, B.L. Zhang, Y.Z. Zhao, Nanoscale 8 (2016) 14222–14236.
[15] Y. Ma, J. Xia, C. Yao, F. Yang, S.G. Stanciu, P. Li, Y. Jin, T. Chen, J. Zheng, G. Chen, H. Yang, L. Luo, A. Wu, Chem. Mater. 31 (2019) 7255–7264.
[16] G.C. Brainard, R. Kavet, I. Kheifets, J. Pineal Res. 26 (1999) 65–100.
[17] S.S. Zhu, X.L. Xu, R. Rong, B. Li, X. Wang, Toxicol. Res. 5 (2016) 97–106.
[18] X. Liang, X. Wang, J. Zhuang, Y.T. Chen, D.S. Wang, Y.D. Li, Adv. Funct. Mater. 16 (2006) 1805–1813.
[19] C. Shi, S.A. Khan, K.P. Wang, M. Schneider, Int. J. Pharm. 479 (2015) 41–51.
[20] Y.Z. Xia, X.X. Wu, J.T. Zhao, J.S. Zhao, Z.H. Li, W.Z. Ren, Y.C. Tian, A.G. Li, Z.Y. Shen, A.G. Wu, Nanoscale 8 (2016) 18682–18692.
[21] Y. Ma, J. Xia, C. Yao, F. Yang, S.G. Stanciu, P. Li, Y. Jin, T. Chen, J. Zheng, G. Chen, Chem. Mater. 31 (2019) 7255–7264.

[22] C. He, Y. Hu, L. Yin, C. Tang, C. Yin, Biomaterials 31 (2010) 3657–3666.
[23] K.Y. Win, S.-S. Feng, Biomaterials 26 (2005) 2713–2722.
[24] B. Dubertret, M. Calame, A.J. Libchaber, Nat. Biotechnol. 19 (2001) 365–370.
[25] L. Josephson, M.F. Kircher, U. Mahmood, Y. Tang, R. Weissleder, Bioconjugate Chem. 13 (2002) 554–560.
[26] T.R. Sathe, A. Agrawal, S.M. Nie, Anal. Chem. 78 (2006) 5627–5632.
[27] F. Wang, Y.C. Wang, S. Dou, M.H. Xiong, T.M. Sun, J. Wang, ACS Nano 5 (2011) 3679–3692.
[28] A. Sangtani, E. Petryayeva, K. Susumu, E. Oh, A.L. Huston, G. Lasarte-Aragones, I.L. Medintz, W.R. Algar, J.B. Delehanty, Bioconjugate Chem. 30 (2019) 525–530.
[29] B.J. Trock, F. Leonessa, R. Clarke, J. Natl. Cancer Inst. 89 (1997) 917–931.
[30] S. Sen, S. Subramanian, D.E. Discher, Biophys. J. 89 (2005) 3203–3213.
[31] D.J. Muller, J. Helenius, D. Alsteens, Y.F. Dufrene, Nat. Chem. Biol. 5 (2009) 383–390.

[32] S.W. Wang, E.A. Konorev, S. Kotamraju, J. Joseph, S. Kalivendi, B. Kalyanaraman, J. Biol. Chem. 279 (2004) 25535–25543.
[33] B. Kalyanaraman, J. Joseph, S. Kalivendi, S.W. Wang, E. Konorev, S. Kotamraju, Mol. Cell. Biochem. 234 (2002) 119–124.
[34] C. Shi, C. Thum, Q. Zhang, W. Tu, B. Pelaz, W.J. Parak, Y. Zhang, M. Schneider, J. Control. Release 237 (2016) 50–60.
[35] Z.T. Liang, Y. Guan, G. Liu, R. Bian, X.B. Zhang, Y. Xiong, Y.C. Tian, Reconstruction of limited-angle and few-view nano-CT image via total variation iterative reconstruction, in: B. Lai (Ed.), X-Ray Nanoimaging: Instruments and Methods, Spie-Int Soc Optical Engineering, Bellingham, 2013.
[36] M. Chen, J. Wu, P. Ning, J. Wang, Z. Ma, L. Huang, G.R. Plaza, Y. Shen, C. Xu, Y. Han, M.S. Lesniak, Z. Liu, Y. Cheng,Small (Weinheim an der Bergstrasse, Germany) (2019) e1905424.